Analysis of the mechanical behaviour of plastic overmolding with metallic inserts

Gabriel Nunes

gabrielnevesnunes@gmail.com

Instituto Superior Técnico, Universidade de Lisboa, Portugal

January 2021

Abstract

The mechanical behaviour of a component obtained by overmolding cannot be correctly analyzed through a structural simulation without considering its mechanical properties and the geometric changes resulting from the injection moulding process. In addition to the consequences arising from the manufacturing process, it must be taken into account that short fiber reinforced polymers have an anisotropic behaviour. Therefore, there is a need for this type of information to be assigned to the material, such as the mapping of the residual strains and fiber orientation obtained at the end of the injection analysis. In the structural analysis of components obtained by overmolding, it is also crucial to define a contact behavior between the different materials in order to get closer to the computational simplifications for a highly complex polymer/metal contact.

In this work the experimental study of a set of components obtained by overmolding is performed considering three types of metal inserts and the time after obtaining the components, aiming to obtain the metal/polymer separation force in uniaxial tensile mode. It is also carried out a study for the numerical reproduction of the physical phenomena evidenced experimentally. To simulate the injection process *Moldflow* was used, while the structural analysis was performed by *Abaqus*. The mapping of the information from *Moldflow* to *Abaqus* and the mechanical characterization of the polymer was executed by Helius PFA. The numerical analysis aimed to reproduce the experimental curves, to validate the mapped information and to verify an approximate polymer/metal contact behaviour regarding the experimental cases.

Keywords: Overmolding; *Moldflow*; Residual Strains; Fiber Orientation; *Abaqus*; *Helius PFA*; Separation Force; Contact Model

1. Introduction

The development of the polymer industry has allowed the substitution of metallic parts by plastic parts, fiber-reinforced plastic parts, and hybrid parts like components obtained by insert overmolding. In this type of injection overmolding an insert of any material is placed into the mold to be covered by the polymer.

The development of polymeric components produced by injection overmolding has become faster, more accurate and cheaper, with the emergence of computational technologies that allow to simulate the various stages of the process. The interaction between this type of software and structural software made it possible to combine the results from the injection phase to the components' in-service phase. However, there is a need to resort to simplifications because it is not always possible to represent all physical phenomena correctly.

The plastic injection process is responsible for inducing residual stresses in the components, having a significant importance in the quality of the product obtained. On the other hand, fiber reinforced polymer injection molding is a complex process due to the anisotropic response of the material, where the mechanical and thermal properties are dependent on the fiber alignment pattern. Therefore, it will be necessary to evaluate and export the results of residual strains and fiber orientation from plastic injection analysis to structural analysis.

The mapping of the injection analysis results will be performed by *Advanced Material Exchange* (AME), a tool of the *Helius PFA* software. It is also possible to characterize a non-linear material by entering experimental data obtained in uniaxial tensile tests such as stress, strain, orientation, temperature, relative humidity and strain rate.

Based on the representation of complex physical phenomena in computational models, the study of components obtained by injection overmolding lacks the assignment of reasonable contact behavior for the different parts. Therefore, there is a need to study real physical phenomena to assign computational behaviors that most faithfully represent what is happening.

This study aims to analyze a set of components obtained by insert overmolding in three types of metal inserts (metal inserts without hole and metal inserts with circular and oblong hole). The study will evaluate their performance regarding the influence of time on the polymeric degradation and the separation force value of the metal insert from the plastic shell in uniaxial tensile regime. In addition, the study also aims to reproduce in a structural analysis software the physical phenomena involved in the separation of the metallic insert. So, it will be conducted an analysis concerning the injection overmolding process by *Moldflow* and the mapping of the residual strains and fiber orientation pattern by AME. Next, it will be introduced the data concerning the response of the nonlinear material in tensile regime. Finally, a structural analysis will be performed by *Abaqus*, aiming to reproduce the curves obtained during the experimental tests.

2. Study Methodology

2.1 Experimental Methodology

In this study, a set of specimens obtained by plastic overmolding with three types of metallic inserts was designed in order to evaluate their performance in uniaxial tensile tests, evaluating the load necessary to separate the metallic insert from the plastic shell. The tensile tests were performed with an universal testing machine, Instron 5966, at a constant crosshead speed of 2 mm/min, and started one week after the specimens were obtained. The specimens shown in Figure 2.1 were labeled as P1, P2, P3, and PP. The polymeric material is a polyamide reinforced with 35% of glass fiber (PA A218 V35 Noir 21N Black) and the metallic insert is a HSLA steel (HX 340 LAD Z275 MBO) with 1 mm thickness.

The P1 specimens are exclusively composed by plastic and were tested experimentally over three weeks, with the objective of studying the influence of time on the mechanical behavior of the material. The P2 specimens were obtained by injection overmolding in three types of metallic inserts (without hole and with circular and oblong hole) with the goal of analyzing the "sandwich" performance of the polymer-metal set. These experimental tests were conducted during two consecutive weeks, through the allocation of the chucks in the polymeric parts. The P3 specimens were obtained by injection overmolding in the three types of metal inserts. The study aimed to evaluate the separation of the metal insert from the polymeric shell. These tests took place over three weeks with the allocation of the upper chuck on the metal part.

PP specimens of type 1BA were obtained in according to the ISO 527-2: 1996 standard. The specimens were machined from injected polymeric plates which were produced through a fan gate design, allowing to obtain specimens with fibers aligned at 0°, 45°, and 90° degrees with the injection direction. The objective of these

experimental tests was to characterize the anisotropic mechanical behavior of the polymer.

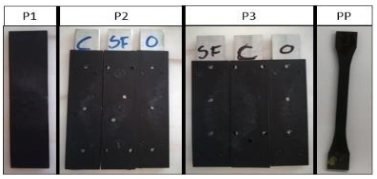

Figure 2.1 – *P1, P2, P3 and PP specimens (SF – without hole; C – circular hole; O – oblong hole)*

2.2 Numerical Methodology

To reproduce the insert metal separation from the polymer envelope carried out on P3 specimens, it is important to consider all the effects that come from the process of injection overmolding. Therefore, it is important to consider the effect of residual stresses on the components obtained, since they are causes of warping and contribute to a less desired performance. On the other hand, the orientation of the fibers influences the mechanical behavior of the material since the maximum loads allowed are conditioned by their orientation. The injection overmolding analysis will be performed by *Moldflow* software and the mapping of the information regarding the residual strains and the orientation of the fibers will be done by AME. In addition, it will be introduced the mechanical behaviour of the polymer characterized during the PP specimens' experimental tests. The structural analysis will be conducted by *Abaqus* through the application of boundary conditions consistent with the experimental tests. However, it will be necessary to define a contact model for the metal/polymer surfaces and the definition of an initial step that allows the reproduction of the effects of the residual stains after the injection process.

2.1.1 Injection Analysis – *Moldflow*

The plastic injection molding process is responsible for generating residual stresses in the components. The residual stresses are stresses that remain in the component in conditions where there are no external loads applied, which has an influence on the performance of the component. It is also one of the causes of volumetric contraction and warping. Due to limitations in computational calculations, *Moldflow* considers the part to always be restricted by the mold, so it has boundary conditions to perform the calculations, therefore the data obtained is related to the in-cavity stresses and deformation. There are two types of residual stresses: the thermally induced residual stresses and the flow induced residual stresses [1].

The thermally induced residual stresses are the result of temperature gradients in the part as it cools and shrinks. The flow induced residual stresses develop during the filling phase and are the result of the physical phenomena of contact between layers of material with different fiber orientation.

First, the CAD files of the three P3 specimens were imported, consisting in the assembly of two parts. Thus, the property of "insert" was attributed to the metal parts, as well as the introduction of mechanical and thermal properties to the material used. A material similar to the real one was introduced for the polymeric part because it did not exist in the software database. The chosen material is called Technyl A218 HPX V3 Black 21N. The data obtained in the experimental tests of PP specimens were also added to characterize the polymer in tensile regime.

Then, meshes were created for the models, as well as the running and cooling systems, according to the components of the molds. The processing conditions were introduced with the same parameters used to obtain the P3 specimens. Finally, a filling + cooling + packing + warping analysis was performed.

As previously mentioned, the results of the deformations and fiber orientation were taken into account, since these data will be exported for structural analysis. The deformations are obtained in the warping analysis and are the direct cause of the residual strains. The conjunction of the fiber orientation with the maximum admitted load allows to calculate the maximum admitted stress for each element of the mesh, which takes great importance in the structural analysis.

2.1.2 Structural Input File – *Abaqus*

2.2.2.1 Mesh and Materials

Before the *Moldflow* information is mapped to *Abaqus* there is a need to create an input structural file to be imported into AME. Initially, it was generated a mesh for the P3 specimen models, with an overall mesh size of 1 mm. Then two sections were created: envelope and insert.

The envelope has been assigned a plastic material with no properties, since they will be introduced in the AME software through experimental data obtained from PP specimens with fibers aligned at 0°, 45°, and 90°. It was

assigned a metallic material to the insert with properties referring to Young's module, Poisson coefficient, and density. Since there is a lack of data representing the material's plastic behavior, a very similar material was found in the bibliography allowing Holloman - Ludwig method application as represented in Equation 2.1 and Table 2.1.

	HX 340 LAD Z 275 MBO	HSLA 350
YIELD STRESS (MPA)	340 - 420	350
MAX. STRESS (MPA)	410 - 510	450
ELONGATION (%)	21	23
n_{enc}	-	0.14
$\mathrm{K_{hl}}$	-	807

$$\sigma_{eff} = \mathrm{K}_{hl}\ {\varepsilon_{eff}}^{\mathrm{n}_{enc}} \tag{2.1}$$

Table 2.1 – *Properties of steels considered to the insert material*

2.2.2.2 Contac Model

The *General Contact* model was chosen to represent the metal/polymer interaction, which gives the same properties for all surfaces in contact. This option prevents penetration due to the interaction between any pair of surfaces. It also corrects the position of the contact interface nodes if they aren't within the admissible penetration tolerance. After choosing the contact model it is necessary to assign properties to it. A mechanical interaction was chosen with emphasis on normal and tangential behavior.

Softened Contact was applied to represent the normal behaviour between surfaces. This model allows some penetration of one surface in the other, being necessary to define the evolution of the contact pressure with the overclosure. After a set of experiments in which were tested different parameters the data introduced are presented in Table 2.2.

Table 2.2 – *Normal Behaviour Definition*

Overclosure (mm)	Pression (Mpa)
0	0
0.1	15
0.5	150

A friction coefficient of 0.6 was chosen to define the tangential behavior. This behaviour is based on Coulomb's theory that relates the maximum shear stress allowed for a section with the contact pressure.

2.2.2.3 Step Definition

Two sequences of analysis were defined to simulate the experimental tests: *step-0* and *step-1*.

The purpose of *step-0* is to obtain the deformations from *Moldflow* through a static step, where the effects of the mapped residual strains are reproduced. This is a non-linear problem, so it is essential that the software decomposes the solicitations in function of the time increment. Therefore, *Abaqus* uses the Newton method to determine an acceptable solution.

Usually, non-linear problems are unstable by transferring the deformation energy from one part of the model to the surrounding parts. Therefore, *Abaqus* uses an automatic mechanism to stabilize quasi static problems through the introduction of a damping coefficient, which can be defined by the user, or established through energy dissipation [46]. So, a body is in balance when the following relationship is satisfied:

$$P - I - F_v = 0 \tag{2.2}$$

where

$$F_v = cM^*v \tag{2.3}$$

P represents the external forces applied, I represents the internal forces and F_v corresponds to the energy dissipated during the deformation making possible the elimination of the effects of rigid body movement. The constant c is the damping coefficient, M^* is an artificial mass matrix calculated with unit density and v is the vector of nodal velocities [2].

Abaqus calculated the damping coefficient since the software assumes that the dissipated energy fraction assumes the default value of 0.0002.

After the *step-0* is configured, *step-1* is defined which represents the tensile test performed to P3 specimens.

2.2.2.4 Boundary Conditions

In order to replicate the experimental test, the base of the polymeric part was encastrated and the upper zone of the metallic part was configured to move at the speed of 2 mm/min. The illustration of the imposed conditions is presented in the Figure 2.2.

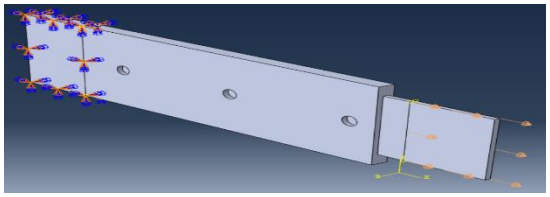

Figure 2.2 – *Boundary Conditions Applied to P3 Specimens*

2.1.3 Mapping Data – Helius PFA

Helius PFA is the software that enables the mapping of data from polymeric injection analysis to structural analysis, through the AME tool. Based on the response of short fiber reinforced polymeric materials, AME was developed so that only the fibers do not present plasticity and rupture, that the nonlinearities are only due to the matrix, and that the plasticity and rupture are highly dependent on the level of fiber alignment.

2.2.2.1 Homogenization and Decomposition Processes

During a structural level finite element simulation of mechanical loading of the short fiber filled plastic, the predicted deformation of the part is based on the stiffness of the homogenized composite material. However, in order to predict plasticity and rupture of the matrix material, *Helius PFA* must decompose the finite element code's homogenized composite strain into the average strain in the matrix constituent material [3].

In the homogenization process of the multiscale material model, the individual constituent properties are input into an incremental Mori-Tanaka micromechanical model that can accommodate evolving matrix properties. The incremental Mori-Tanaka micromechanics model produces homogenized composite properties for the idealized, perfectly aligned material. These properties, in turn, are operated upon by the fiber orientation tensor to produce the homogenized composite properties for the real material with the actual fiber orientation distribution [4].

The decomposition process maps homogenized composite strain increments into the average strain increments in the plastic matrix constituent material. The decomposition process makes use of the instantaneous constituent properties, the incremental Mori-Tanaka micromechanics model, and the fiber orientation tensor. The computed average strain increment in the matrix constituent is used to drive the matrix plasticity model and predict the evolution of the matrix tangent modulus [5].

2.2.2.2 Plasticity Model

The response of the matrix constituent material is provided by a Ramberg-Osgood plasticity model that has been enhanced to allow the predicted plastic response to exhibit sensitivity to the direction of the loading relative to the fiber direction. For short fiber filled plastics that have a high degree of fiber alignment, the degree of plasticity exhibited prior to final rupture will depend strongly upon the direction of the loading relative to the average direction of the reinforcing fibers. The Ramberg-Osgood model can easily be enhanced to accommodate directional dependency. To do so, the form of the effective Von Mises stresses is modified, as shown below:

$$\sigma_{eff} = \sqrt{\frac{(\alpha\sigma_{11}-\beta\sigma_{22})^2+(\beta\sigma_{22}-\beta\sigma_{33})^2+(\beta\sigma_{33}-\alpha\sigma_{11})^2+6[(\sigma_{12})^2+(\sigma_{23})^2+(\sigma_{31})^2]}{2}} \quad (2.4)$$

where α and β are weighting coefficients used to differentiate the impact of stress components in the average fiber direction compared to stress components that are normal to the average fiber direction [6].

2.2.2.3 Rupture Model

The MCT method is the default rupture model used by AME. In the MCT method, we assume the matrix rupture criterion is expressed as a quadratic function of the matrix average stress components.

$$I_1^m = \sigma_{11}^m \quad (2.5)$$

$$I_2^m = \sigma_{22}^m + \sigma_{33}^m \quad (2.6)$$

$$I_4^m = (\sigma_{12}^m)^2 + (\sigma_{13}^m)^2 \quad (2.7)$$

$$\pm A_1^m (I_1^m)^2 \pm A_2^m (I_2^m)^2 + A_4^m I_4^m \geq 1 \quad (2.8)$$

The quantities A_i^m are the adjustable coefficients of the matrix failure criteria that must be determined from tensile tests for the 0°, 45° e 90° data sets [7].

2.2.2.4 Mapping Analysis

The mapping analysis is initiated by importing the injection file (.sdy) and the structural file (.inp). Then, the alignment of the two models is performed, so that the mapping is done correctly.

After the model alignment, the data characterizing the polymeric material that were obtained in the uniaxial tensile tests of the PP specimens for the three fiber directions must be

introduced.

Finally, the data are mapped from the injection model to the structural model. However, first the *Mapping Suitability Plot* tool should be used in order to verify sufficient refinement between meshes. After the mapping, the files are exported to the structural analysis.

3. Results

3.1 Experimental Results

3.1.1 P1 Specimens

P1 specimens obtained by polymeric injection molding were experimentally tested on July 2020 days 7,14, and 21. The results of the uniaxial tensile tests are presented in Figure 3.1 along with the amplification in the initial stages. It is verified that the obtained curves present an initial slope, which may indicate a relaxation of the residual stresses as the uniaxial tensile test occurs. On the other hand, the loss of the initial slope may indicate that there is a relief of the residual stresses over time.

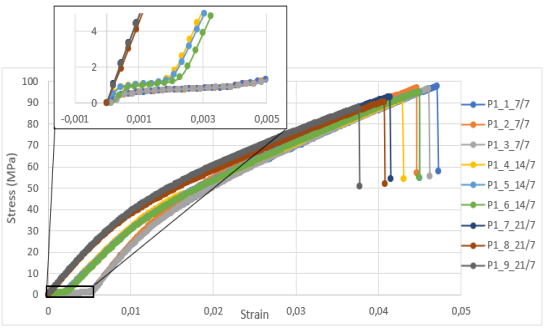

Figure 3.1 – *Nominal Stress – Strain Curves Obtained for P1 Specimens*

3.1.2 P2 Specimens

P2 specimens obtained by polymeric injection overmolding were experimentally tested on July 2020 days 14 and 21. The results of the uniaxial tensile tests to P2_SF, P2_C, and P2_O are presented in Figure 3.2, Figure 3.3, and Figure 3.4, respectively, along with the amplification in the force decay zones. Regardless of the type of insert, the maximum force values are similar to each other. This is due to the fracture of the polymeric material, which is the first to break. It is also possible to verify a suddenly decay value of the force during the experimental tests, which is associated with the separation of the plastic and metal surfaces. On the other hand, the decay of the force value is more significant for the specimens without holes (P2_SF), since the polymer/metal adhesion forces are the only ones that restrict the relative position between the parts. Finally, it was verified that the force decay occurs for lower force and displacement values in the second week, indicating a loss of polymer/metal adhesion over time.

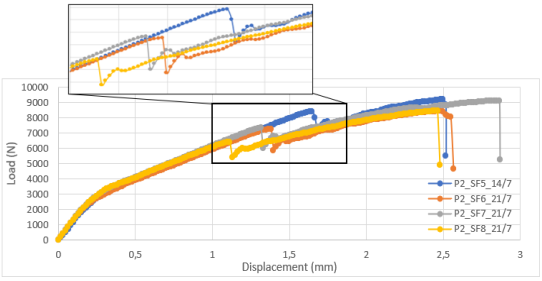

Figure 3.2 – *Load – Displacement Curves Obtained for P2_SF Specimens*

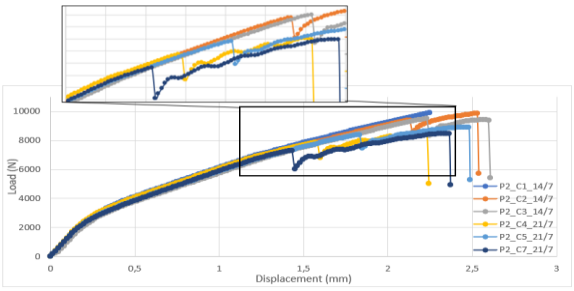

Figure 3.3 – *Load – Displacement Curves Obtained for P2_C Specimens*

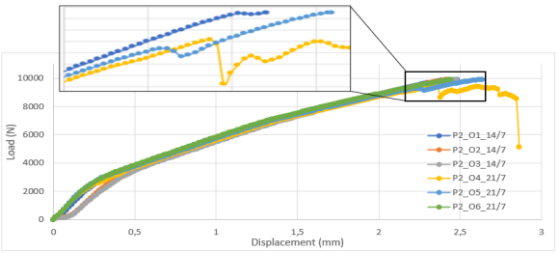

Figure 3.4 – *Load – Displacement Curves Obtained for P2_O Specimens*

3.1.3 P3 Specimens

P3 specimens obtained by polymeric injection overmolding were experimentally tested on July 2020 days 7,14, and 21. The results of the uniaxial tensile tests to P3_SF, P3_C, and P3_O are presented in Figure 3.5, Figure 3.6, and Figure 3.7, respectively, along with the amplification in the force increase zones. Higher force values are reached for the specimens whose inserts have holes (P3_C and P3_O). Likewise, the displacement values at the maximum force points are also higher for the test specimens whose inserts have holes. This is due to the existence of polymeric material in the hole zone that imposes higher loads so that the metal part is separated from the polymeric part. On the other hand, the values are relatively higher for

oblong holes than for circular holes, since the amount of polymeric volume in the hole zone influences the necessary load to reproduce the same effects.

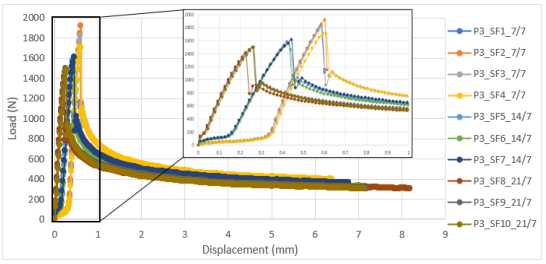

Figure 3.5 – *Load – Displacement Curves Obtained for P3_SF Specimens*

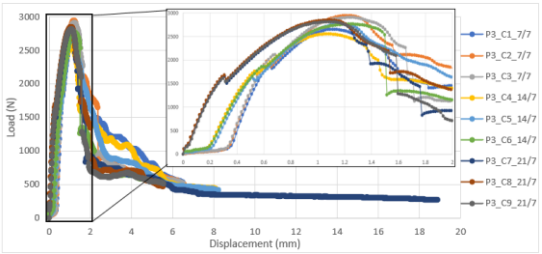

Figure 3.6 – *Load – Displacement Curves Obtained for P3_C Specimens*

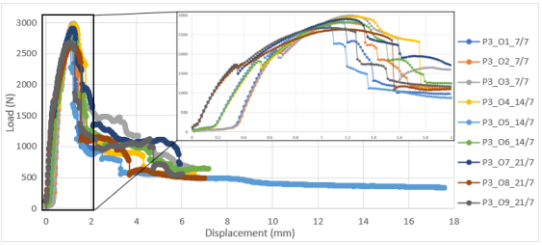

Figure 3.7 – *Load – Displacement Curves Obtained for P3_O Specimens*

Like the P1 tests specimens, the initial slopes were also obtained, as shown in Figure 3.8. Likewise, this slope indicates the relief of residual stresses in the initial phase of the experimental tests. On the other hand, the loss of the initial slope indicates the relief of the residual stresses over time.

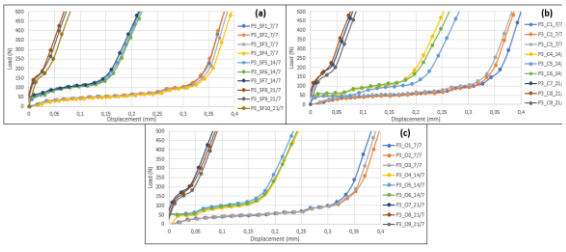

Figure 3.8 – *Load – Displacement Curves with the Initial Slopes Obtained for P3 Specimens: (a)P3_SF; (b)P3_C; (c)P3_O*

Based on the obtained results, two types of curves can be built for the separation tests in uniaxial tensile regime, as shown in Figure 3.9. Graph – I is a typical separation curve for metal inserts without holes, while Graph – II displays a typical separation curve for inserts with holes.

In Graphic – I, **point – a** corresponds to the separation of the metallic insert surfaces from the polymeric part. Then, the force value decreases abruptly, corresponding to the slipping of the insert along the internal walls of the polymeric part, submitted only to the existing friction. In Graph – II, **point – b** corresponds to the separation of the surfaces of the insert from the polymeric part. The increase of the force value up to **point – c** is caused by the resistance that the plastic material in the insert hole region causes to the movement of the insert. As soon as the plastic material in the hole yields, the force decreases, and the insert is separated from the polymeric part.

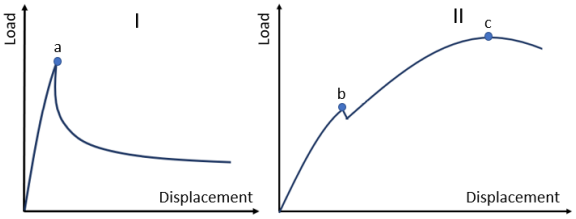

Figure 3.9 – *Typical Separation Curves in Uniaxial Tensile Regime: (I)Inserts without holes; (II)Inserts with holes*

The graph in Figure 3.10, enables to evaluate the adhesion between the polymeric and metallic surfaces. The graph presents the separation values obtained for each specimen and its evolution throughout the experimental tests. This means that it corresponds to the **point – a** value of Figure 3.9 Graph–I, for the P3_SF specimens, and the **point – b** value of Figure 3.9 Graph – II, for the P3_C and P3_O specimens. It were evaluated the data independently of the initial slope so that the residual stresses had no influence on the analysis performed.

It is possible to verify that for the three specimens types the value of the separation force decreases over time. This is indicative of the loss of adhesion of the surfaces over time.

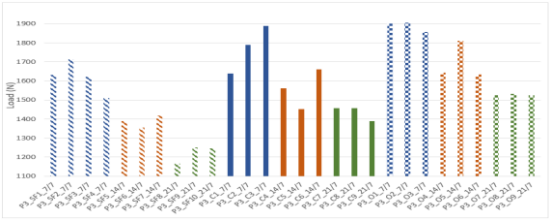

Figure 3.10 – *Evolution of Separation Force over time for the P3 Specimens*

3.1.4 PP Specimens

Machined PP specimens of polymeric plates obtained by injection molding were submitted to uniaxial tensile tests in order to characterize the anisotropic mechanical behaviour of the polymer. These is the data that will be introduced in AME. The results are presented in Figure 3.11, Figure 3.12, and Figure 3.13 for fibers at 0°, 45° and 90°, respectively.

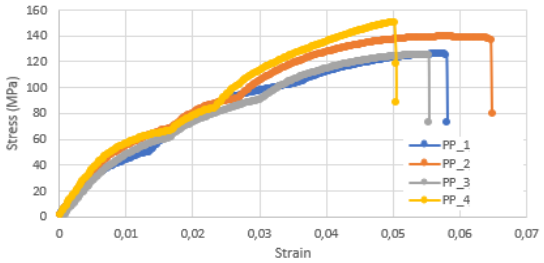

Figure 3.11 – *Stress – Strain Curves Obtained for PP Specimens with Fibers at* 0°

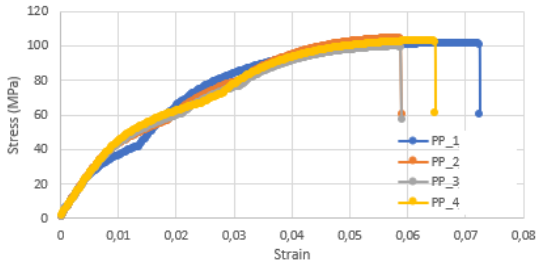

Figure 3.12 – *Stress – Strain Curves Obtained for PP Specimens with Fibers at* 45°

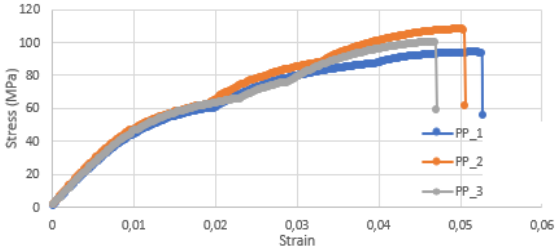

Figure 3.13 – *Stress – Strain Curves Obtained for PP Specimens with Fibers at* 90°

3.2 Numerical Results

3.2.1 STEP – 0

In order to verify the calculation compatibility between software it is necessary to compare the deformations obtained in *Moldflow* and *Abaqus*. For this purpose, Table 3.1 is presented. For all case studies, a significant percentual difference was verified for the obtained minimum deformation values, although the maximum value corresponds to 0.00584 mm. On the other hand, the deformation magnitude maximum values differences of 34% corresponds to 0.12mm.

Table 3.1 – *Quantitative Comparation of the Deformation Between Moldflow and Abaqus*

SPECIMENS	U(MAG) (MM)		DIFFERENCE	
	MIN	MAX	MIN	MAX
P3_SF_MOLDFLOW	0.0008	0.3371	366%	34%
P3_SF_ABAQUS	0.003727	0.4508		
P3_C_MOLDFLOW	0.0013	0.3369	366%	27%
P3_C_ABAQUS	0.006058	0.4274		
P3_O_MOLDFLOW	0.0014	0.3356	417%	22%
P3_O_ABAQUS	0.007239	0.4083		

To qualitatively compare the deformation, Figure 3.14 is shown. The figure concerns the P3_SF specimen. However, the results are similar for P3_C and P3_O specimens. The deformations are very similar between the two software, except for the deformation magnitude of the polymeric zone adjacent to the entrance of the polymeric envelope, in which *Abaqus* considers a significant deformation compared to *Moldflow*.

Figure 3.15 shows the contact status for the insert upper and lower surfaces in the end of *step-0*. It is observed that the most central area is not in contact. However, contact is observed in the surroundings of the insert as well as in the area adjacent to the holes. Therefore, contact is enhanced in places adjacent to the polymeric material intersections of the two opposite faces of the insert.

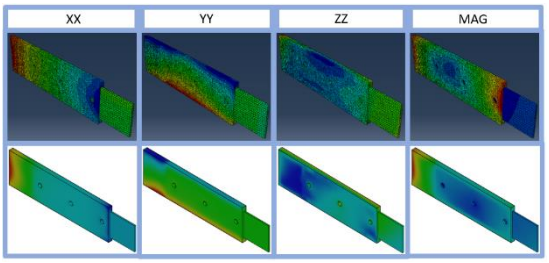

Figure 3.14 – *Qualitative Comparation of the Deformation Between Moldflow and Abaqus*

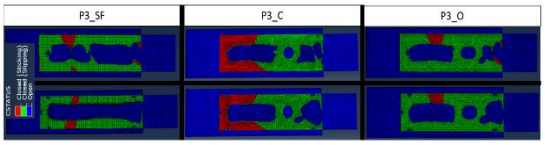

Figure 3.15 – *Contact Status in the end of step-0*

Moldflow calculates Mises - Henchy stresses at the end of the warping analysis, which is mostly due to differences in temperature gradients during cooling, while the component is still constrained by the mold walls. On the other hand, the residual stresses calculated by *Abaqus* are the Von Mises stresses, which values are obtained at the end of the initial step. It was verified that *Abaqus* calculates higher values. However, there is a good compatibility between

the results presented by the two software.

3.2.2 STEP – 1

3.2.2.1 P3_SF Specimen

Figure 3.16 presents the numerical results of the P3_SF specimen along with the experimental results. Although the residual stresses were reproduced in *step-0*, *Abaqus* does not reproduce their relaxation in the initial increments. This may be due to the difference in real and numeric values.

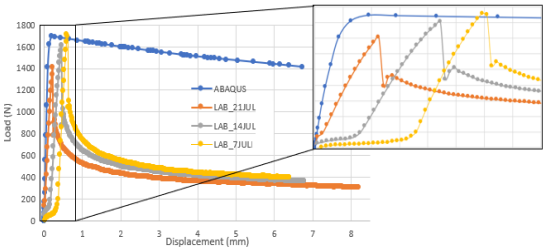

Figure 3.16 – *Numerical and Experimental Load – Displacement Curves Obtained for P3_SF Specimens*

In order to evaluate the numerical model largest slope a simulation was performed in *Moldflow* and *Abaqus* for the P1 specimens. The results are presented in Figure 3.17. Once again, the numerical curve has a higher slope compared to the experimental results. This can be caused by a defective fiber alignment when the PP specimens were obtained. Therefore, the incorrect mechanical characterization of the polymer has a significant influence on the numerical simulation.

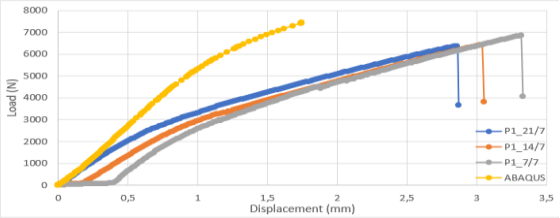

Figure 3.17 – *Numerical and Experimental Load – Displacement Curves Obtained for P1 Specimens*

Despite the stiffness difference of the curves, in Figure 3.16 we observe that the separation force of the insert (1697 N) is very close to the value of the experimental curve of July 7 (1715 N). However, the correspondent displacement value is different.

After the separation force is reached, the experimental curves differ a lot from the numerical curve. Although the numerical curve presents an approximately constant slope in the force decrease phase, the slope is three times higher than the experimental values. Taking into account the non-reproduction of the force value abrupt decline and the slope differences, it can be assumed that the contact conditions do not represent the real physical phenomena.

3.2.2.2 P3_C and P3_O Specimens

Figure 3.18 presents the numerical results of the P3_C and P3_O specimens along with the experimental results. Once again, *Abaqus* does not reproduce the destruction of the residual stresses. Both analyses didn't conclude due to numerical convergence problems.

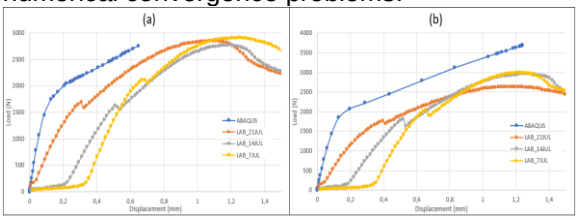

Figure 3.18 – *Numerical and Experimental Load – Displacement Curves Obtained: (a)P3_C Specimens; (b)P3_O Specimens*

Once again, the numerical curves have a bigger slope compared to the experimental curves. As seen previously, the incorrect mechanical characterization of the polymer has significant implications on the numerical analysis.

On the other hand, it is verified that the slope variation occurs for force values close to the experimental models' local maximum, between 1700 N and 1800N, when the metallic insert is separated from the polymer envelope. After the separation of the two materials' interfaces, the slope variation goes along with the experimental curves' tendency. Its force increments are caused by the polymeric material existing in the holes of the inserts. Therefore, the tendencies of the numerical curves are similar to the experimental ones.

Although the tendency is similar in numerical and experimental models, it was observed that the P3_O numerical model increases for much higher force values. This difference may be related to the plasticity and rupture criteria calculated by AME, which allows the material to resist to higher loads. As said before, these problems are consequences of incorrect polymeric characterization.

P3_C and P3_O numerical curves are more similar to the experimental validations than P3_SF. In the P3_SF model it was verified that the contact parameters did not represent the real contact conditions. The same is true for P3_C and P3_O models. However, the difference is related to the plastic material in the insert hole zone, which allows the contact model to become irrelevant. In these cases, it is the polymeric material of the hole that influences the separation of the insert.

4. Conclusions

The destruction of residual stresses in uniaxial tensile tests to polymeric components obtained by injection molding and injection overmolding was verified. It was also observed the deterioration of the residual stresses over time.

Regarding components obtained only by injection overmolding, was verified that in tensile tests carried out to a metal/polymer set, first occurs the separation of the two surfaces and then the fracture of the polymeric part.

In the separation experiments performed in uniaxial tensile regime were observed two types of curves. On a typical curve for an insert without holes, the maximum force corresponds to the separation force of the surfaces. On the other hand, a typical curve for inserts with holes has a local maximum that corresponds to the separation force of the surfaces. Then, the force increases until the rupture of the polymeric material existing at the hole intersection.

For the experimental tests was also verified loss of adhesion of the surfaces in contact over time.

Through data mapping from injection analysis to structural analysis was verified an optimal correspondence between *Moldflow* and *Abaqus*. However, *Abaqus* did not reproduced the destruction of residual stresses at the beginning of the solicitation step. This may be due the differences of numerical and real values.

Abaqus managed to obtain separation forces closely to the experimental values for the P3 specimens. However, they did not occur in the same instants of time.

Finally, an acceptable correspondence in the tendency of the curves for inserts with holes was verified. The same was not true for inserts without holes. Thus, it was concluded that the defined contact model does not represent the real physical phenomena. Although an acceptable tendency for inserts with holes was obtained, this was only due to the polymeric material existing in the hole zone, which made the contact model irrelevant for the numerical operation.

Institutional Acknowledgments

This work was developed in the scope of the project TOOLING4G - Advanced Tools for Smart Manufacturing project, Mobilizer Project No. 24516, Notice No. 10 / SI / 2016, Ref. POCI-01-0247-FEDER-024516, within the scope of PORTUGAL 2020 , and co-financed by the European Union through the FEDER.

References

[1] SOUSA, J. Integration of residual stresses and deformations induced by the injection molding process in structural finite element simulation of polymeric components. Tese de Mestrado, Instituto Superior Técnico, Universidade de Lisboa (2015).

[2] Abaqus – User's Guide, URL: http://130.149.89.49:2080/v6.11/books/usb/default.htm, accessed in October 2020

[3] Autodesk Helius PFA – Theory Manual, URL: http://help.autodesk.com/view/ACMPAN/2017/ENU/?guid=GUID-7776FA5F-EBA5-4F09-A06B-639AEF847D7B, accessed in June 2020

[4] Autodesk Helius PFA – Theory Manual, URL: http://help.autodesk.com/view/ACMPAN/2017/ENU/?guid=GUID-4211DF13-5CF3-4D0A-9ED8-E7D683BEED17, accessed in June 2020

[5] Autodesk Helius PFA – Theory Manual, URL: http://help.autodesk.com/view/ACMPAN/2017/ENU/?guid=GUID-AF01F76F-53A4-4C27-9498-6765075932B6, accessed in June 2020

[6] Autodesk Helius PFA – Theory Manual, URL: http://help.autodesk.com/view/ACMPAN/2017/ENU/?guid=GUID-F156C59C-37BE-437C-AD98-CD40B72BB89C, accessed in June 2020

[7] Autodesk Helius PFA – Theory Manual, URL: http://help.autodesk.com/view/ACMPAN/2017/ENU/?guid=GUID-144B8416-8216-45C7-A2A0-3889DC2CE373, accessed in June 2020